Journal of Turbulence

ISSN: (Print) 1468-5248 (Online) Journal homepage: http://www.tandfonline.com/loi/tjot20

Large eddy simulation of orientation and rotation of ellipsoidal particles in isotropic turbulent flows

Jincai Chen, Guodong Jin & Jian Zhang

To cite this article: Jincai Chen, Guodong Jin & Jian Zhang (2016) Large eddy simulation of orientation and rotation of ellipsoidal particles in isotropic turbulent flows, Journal of Turbulence, 17:3, 308-326, DOI: 10.1080/14685248.2015.1093638

To link to this article: http://dx.doi.org/10.1080/14685248.2015.1093638

JOURNAL OF TURBULENCE, 2016
VOL. 17, NO. 3, 308–326
http://dx.doi.org/10.1080/14685248.2015.1093638

Taylor & Francis
Taylor & Francis Group

Large eddy simulation of orientation and rotation of ellipsoidal particles in isotropic turbulent flows

Jincai Chen, Guodong Jin and Jian Zhang

State Key Laboratory of Nonlinear Mechanics, Institute of Mechanics, Chinese Academy of Sciences, Beijing, China

ABSTRACT

The rotational motion and orientational distribution of ellipsoidal particles in turbulent flows are of significance in environmental and engineering applications. Whereas the translational motion of an ellipsoidal particle is controlled by the turbulent motions at large scales, its rotational motion is determined by the fluid velocity gradient tensor at small scales, which raises a challenge when predicting the rotational dispersion of ellipsoidal particles using large eddy simulation (LES) method due to the lack of subgrid scale (SGS) fluid motions. We report the effects of the SGS fluid motions on the orientational and rotational statistics, such as the alignment between the long axis of ellipsoidal particles and the vorticity, the mean rotational energy at various aspect ratios against those obtained with direct numerical simulation (DNS) and filtered DNS. The performances of a stochastic differential equation (SDE) model for the SGS velocity gradient seen by the particles and the approximate deconvolution method (ADM) for LES are investigated. It is found that the missing SGS fluid motions in LES flow fields have significant effects on the rotational statistics of ellipsoidal particles. Alignment between the particles and the vorticity is weakened; and the rotational energy of the particles is reduced in LES. The SGS-SDE model leads to a large error in predicting the alignment between the particles and the vorticity and over-predicts the rotational energy of rod-like particles. The ADM significantly improves the rotational energy prediction of particles in LES.

ARTICLE HISTORY
Received 6 June 2015
Accepted 25 August 2015

KEYWORDS
Fibres; rotational dynamics; large eddy simulation; subgrid scale model; approximate deconvolution method

1. Introduction

The dynamics of ellipsoidal particles suspended in turbulence is a central problem in many engineering applications and natural environmental flows. For examples, in marine biology, the dynamics of small planktonic organisms suspended in the ocean is a fundamental problem in understanding their feeding and breeding patterns;[1–3] in paper making, the rotational dispersion of fibres plays an important role. The orientational distribution dominates the mechanical and other properties of the finished paper.[4] When the fibres are

CONTACT Guodong Jin gdjin@lnm.imech.ac.cn

oriented primarily in one direction, the paper will be strong in that direction, which is suitable for newsprint. However, high-quality papers, such as magazine or laser printer papers, require an isotropic orientational distribution.

Jeffery [5] studied the rotational motion of small ellipsoidal particles in a fluid flow, and proposed an equation of motion for the direction of the long-axis vector $\boldsymbol{p}$ governed by the fluid velocity gradient tensor. Bretherton [6] extended Jeffery's equation with a shape parameter, the aspect ratio $\alpha = l/d$, where l is the length of the ellipsoidal particle and d is the diameter. In this study, ellipsoidal particles are generally referred to as rod- or disk-like particles, as determined by α; $\alpha \ll 1$ corresponds to a flat, disk-like particle, $\alpha = 1$ corresponds to a spherical particle, and $\alpha \gg 1$ corresponds to an elongated, rod-like particle. Recently, the dynamics of ellipsoidal particles in turbulent flows have been extensively studied.[7–14] However, the study on the orientational and rotational dynamics of ellipsoidal particles in the context of large eddy simulation (LES) is relatively scarce.

In recent years, LES has become a successful tool in the computational fluid dynamics software [15] in predicting single-phase turbulent flows and particle-laden turbulence,[16–19] the latter requires that LES is time accurate.[20–22] In conventional LES, the large-scale turbulent motions are explicitly resolved, whereas the effects of the subgrid scale (SGS) motions are modelled. Because the mesh resolution employed in LES is much coarser than that used in direct numerical simulation (DNS), LES is more economical than DNS and can be applied to turbulent flows at high Reynolds numbers. However, if we replace the real fluid velocity with the resolved scale velocity to compute the fluid velocity gradient tensor experienced by small, rigid fibres without considering the effects of the SGS velocity, it will introduce large errors into the rotational statistics of fibres according to Jeffery's equation. In addition, the rotational dispersion coefficient of the ellipsoidal particles is related to the turbulent energy dissipation rate,[23] which is reduced in LES because of the lack of SGS fluctuations. Thus, the effect of the SGS motions of fluid velocity on the rotational motion of ellipsoidal particles is an important and open issue.

To model the effects of the unresolved SGS fluid motions on the dispersion of spherical inertial particles, two types of models for particles have been developed. The first one is a Langevin-type model for SGS motions, where the missing fluctuations can be compensated by stochastic information [24,25] based on a stochastic differential equation (SDE). The second one is based on the approximate deconvolution method (ADM),[26–28] where the energy spectrum near the cut-off number is recovered to some extent.[29] Michałek et al. [30] proposed a hybrid stochastic-deconvolution model for particles in LES of particle-laden turbulence by combining the SDE and the ADM.

The motion of inertialess ellipsoidal particles is much more complicated than that of spherical particles due to the three additional rotational degrees of freedom. The translational motion is controlled by large-scale motions, whereas the rotational motion is determined by the fluid velocity gradient tensor at small scales. Therefore, the LES of the orientational and rotational statistics of the ellipsoidal particles in turbulence encounters new challenges due to the lack of SGS motions. Therefore, our objectives are to examine the effects of SGS motions and further to assess the performances of SGS models on the prediction of orientational and rotational statistics of ellipsoidal particles.

This paper is organised as follows. The governing equations for fluid and particle motions are provided in Section 2. The validation of our simulation results, the alignment of the rod- and disk-like particles with the vorticity and the Lagrangian fluid stretching direction, the effects of the missing SGS motions and the performance of SGS models on

the rotational statistics of ellipsoidal particles, are presented in Section 3. Conclusions are provided in Section 4.

2. Numerical simulations

We consider the motion of rigid, inertialess and ellipsoidal particles smaller than the Kolmogorov length scale in isotropic turbulent flows. The particle concentration is very dilute, so the one-way coupling from fluid to particles is assumed, and collisions between particles are neglected. In this section, the governing equations for turbulent flows and particle motions are presented.

2.1. Flow field

2.1.1. DNS method

The DNS of isotropic turbulence is performed using a pseudo-spectral method in a box of $(2\pi)^3$, which is discretised into N^3 grid points ($N = 128$ and 512 in this paper). The Navier–Stokes equations for incompressible isotropic turbulence in spectral space can be represented as ($|\boldsymbol{k}| < k_{\max}$)

$$\left(\frac{\partial}{\partial t} + \nu k^2\right)\hat{\boldsymbol{u}}(\boldsymbol{k}, t) = \boldsymbol{P}(\boldsymbol{k})\mathcal{F}(\boldsymbol{u} \times \boldsymbol{\omega}) + \hat{\boldsymbol{f}}(\boldsymbol{k}, t), \tag{1}$$

where $\boldsymbol{u}$ and $\hat{\boldsymbol{u}}(\boldsymbol{k}, t)$ are the fluid velocities in physical and spectral space, respectively. $k_{\max}$ is the maximum cut-off wavenumber, $k_{\max} = N/3$. $\boldsymbol{k} = (k_1, k_2, k_3)$ is the wavenumber vector, with $k = |\boldsymbol{k}|$, $\boldsymbol{\omega} = \nabla \times \boldsymbol{u}$ is the vorticity in physical space, and ν is the fluid kinematical viscosity. The projection tensor $\boldsymbol{P}_{jm} = \delta_{jm} - k_j k_m / k^2$ ($j, m = 1, 2, 3$), and $\mathcal{F}$ denotes a Fourier transform. The artificial forcing term $\hat{\boldsymbol{f}}(\boldsymbol{k}, t)$ is used to drive and maintain the turbulent flow using a deterministic forcing scheme.[31,32] The spectral velocity fields are advanced in time using a second-order Adams–Bashforth method for the non-linear term and an exact integration for the linear viscous term. In our simulations, the Courant–Friedrichs–Lewy number is less than 0.5 and $k_{\max}\eta$ is larger than 1.1, where η is the Kolmogorov length scale of turbulent flows.

2.1.2. Filtered DNS (FDNS) velocity fields

The filtered velocity fields can be computed using a filtering operation on the Fourier coefficients from DNS, where the filter used in this paper is a sharp spectral filter $H(k_c - |\boldsymbol{k}|)$ (H is the Heaviside function),

$$\tilde{\boldsymbol{u}}(\boldsymbol{x}, t) = F^{-1}\begin{cases}\hat{\boldsymbol{u}}(\boldsymbol{k}, t) & \text{if } |\boldsymbol{k}| \in [1, k_c], \\ 0 & \text{if } |\boldsymbol{k}| \in (k_c, k_{\max}],\end{cases} \tag{2}$$

where $\tilde{\boldsymbol{u}}(\boldsymbol{x}, t)$ is the filtered velocity in physical space and k_c is the cut-off wavenumber, $k_c = 0.25k_{\max}$ in this paper. The SGS velocity field is then

$$\boldsymbol{u}'(\boldsymbol{x}, t) = \boldsymbol{u}(\boldsymbol{x}, t) - \tilde{\boldsymbol{u}}(\boldsymbol{x}, t). \tag{3}$$

Because FDNS, regarded as an ideal LES, does not introduce any SGS modelling errors into the flow fields, it plays an important role in studying the effects of SGS eddies on the statistics of particle motions.

2.1.3. LES method

The same pseudo-spectral method and forcing scheme as DNS are used in LES. However, it is performed on a much coarser grid, such that the SGS velocity fields are unresolved. The governing equations in LES can be written as

$$\left\{\frac{\partial}{\partial t}+[\nu+\nu_e(k|k_c)]k^2\right\}\hat{\bar{\boldsymbol{u}}}(\boldsymbol{k},t)=\boldsymbol{P}(\boldsymbol{k})\mathcal{F}(\bar{\boldsymbol{u}}\times\bar{\boldsymbol{\omega}})+\hat{\boldsymbol{f}}(\boldsymbol{k},t), \tag{4}$$

where $\bar{\boldsymbol{u}}$ and $\bar{\boldsymbol{\omega}}$ are the filtered fluid velocity and vorticity in physical space, respectively, and $\hat{\bar{\boldsymbol{u}}}$ is the filtered fluid velocity in spectral space. $\nu_e(k|k_c)k^2\hat{\bar{\boldsymbol{u}}}(\boldsymbol{k},t)$ denotes the net dissipative effects of SGS motion on the resolved scale flow. We use the spectral eddy viscosity SGS model [33,34] to close Equation (4),

$$\nu_e(k|k_c)=\nu_e^+(k/k_c)\sqrt{\frac{E(k_c)}{k_c}}, \tag{5}$$

where

$$\nu_e^+(k/k_c)=C_K^{-3/2}[0.441+15.2\exp(-3.03k_c/k)]. \tag{6}$$

In our study, the Kolmogorov constant C_K is 2.0, and $E(k_c)$ is the value of the energy-spectrum function at the cut-off wavenumber k_c.

2.2. Particle motion

The motions of an ellipsoidal particle can be classified into translational and rotational motions. The inertialess ellipsoidal particle is solely convected by the flow, so its translational motion can be described by the fluid velocity at the centre position of an ellipsoidal particle, $\boldsymbol{x}_p(t)$.

When turbulent flow reaches a statistically steady state at t_0, the particles are seeded into the flow field at $\boldsymbol{x}_0$, and the translational motion of an ellipsoidal particle is described by

$$\dot{\boldsymbol{x}}_p(t;\boldsymbol{x}_0,t_0)=\boldsymbol{u}(\boldsymbol{x}_p,t;\boldsymbol{x}_0,t_0), \tag{7}$$

where $\dot{(\,)}$ denotes the Lagrangian time derivative, $\boldsymbol{x}_p(t;\boldsymbol{x}_0,t_0)$ and $\boldsymbol{u}(\boldsymbol{x}_p,t;\boldsymbol{x}_0,t_0)$ are the position and velocity of particles at time t. The Lagrangian velocity $\boldsymbol{u}(\boldsymbol{x}_p,t;\boldsymbol{x}_0,t_0)$ can be obtained from the Eulerian velocity field $\boldsymbol{u}(\boldsymbol{x},t)$ by a six-point Lagrangian interpolation in each spatial direction.[35] Then, we can use a fourth-order Adam–Bashforth method [36] to calculate the displacement of particles.

In this study, the length scale $\max(l,d)$ of the ellipsoidal particles is assumed to be smaller than the Kolmogorov length scale in DNS, and thus, much smaller than the filter length Δ

in LES ($\Delta = \pi/k_c$). Thus, they experience viscous laminar flow at the scales of their length, and their rotational motion can be described using Jeffery's equation,[5]

$$\dot{p}_i = \Omega_{ij} p_j + \frac{\alpha^2 - 1}{\alpha^2 + 1} \left(S_{ij} p_j - p_i p_k S_{kl} p_l \right), \tag{8}$$

where Ω_{ij} is the rate-of-rotation tensor and S_{ij} is the rate-of-strain tensor along the trajectory of the ellipsoidal particle,

$$\Omega_{ij} = \frac{1}{2} \left(\frac{\partial u_i}{\partial x_j} - \frac{\partial u_j}{\partial x_i} \right), \quad S_{ij} = \frac{1}{2} \left(\frac{\partial u_i}{\partial x_j} + \frac{\partial u_j}{\partial x_i} \right), \tag{9}$$

p_i is a component of the orientation vector, and $\alpha = l/d$ is the aspect ratio, which determines the shape factor of an ellipsoidal particle, $\Lambda = (\alpha^2 - 1)/(\alpha^2 + 1)$. The first term on the right-hand side of Equation (8) denotes the rotation rate caused by the vorticity, and the second one denotes the rotation rate caused by the shear strain, where the elongation of $\boldsymbol{p}$ due to the contribution of S_{ij} is subtracted by the non-linear term $p_i p_k S_{kl} p_l$, such that the orientation vector $\boldsymbol{p}$ is constrained to be a unit vector. For a detailed derivation, please refer to Ref. [37].

3. Results and discussion

3.1. Validation of the codes

To validate our codes for capturing the orientational and rotational statistics of ellipsoidal particles, we compared our results with those obtained by Pumir and Wilkinson [9] and Parsa et al.,[10] respectively. First, we consider the alignment of ellipsoidal particles in turbulent flows.

In this study, the alignment of ellipsoidal particles is defined as the cosine of the angle between the orientation vector of the particles, $\boldsymbol{p}$, and the direction vectors, $\boldsymbol{e}_i$, where $\boldsymbol{e}_i$ denotes the three orthonormal eigenvectors $\boldsymbol{e}_1$, $\boldsymbol{e}_2$, $\boldsymbol{e}_3$ of the symmetric matrix $\boldsymbol{S}$ and the unit direction vector $\boldsymbol{e}_\omega$ of the vorticity $\boldsymbol{\omega}$. The eigenvectors of $\boldsymbol{S}$ can be solved from

$$\boldsymbol{S e_i} = \lambda_i \boldsymbol{e}_i, \tag{10}$$

where λ_i, ordered by $\lambda_1 \geq \lambda_2 \geq \lambda_3$, are the eigenvalues of $\boldsymbol{S}$. In addition, the antisymmetric vorticity tensor $\boldsymbol{\Omega}$ corresponds to a vorticity vector $\boldsymbol{\omega}$ by $2\Omega_{ij} = -\epsilon_{ijk}\omega_k$, where ϵ_{ijk} is a permutation tensor with magnitude ω and the unit direction vector $\boldsymbol{e}_\omega$,

$$\boldsymbol{\omega} = (\omega_x, \omega_y, \omega_z) = \omega \boldsymbol{e}_\omega, \quad \boldsymbol{\Omega} = \frac{1}{2} \begin{pmatrix} 0 & -\omega_z & \omega_y \\ \omega_z & 0 & -\omega_x \\ -\omega_y & \omega_x & 0 \end{pmatrix}. \tag{11}$$

It was shown that the statistics characterising the alignment of rod-like particles with $\alpha \to \infty$ are independent of the Reynolds number in the range $45 \leq R_\lambda \leq 170$.[9] We choose $\alpha = 100$ to represent a rod-like particle in our case. Since the second-order moment $\langle (\boldsymbol{p} \cdot \boldsymbol{e}_i)^2 \rangle$ is more sensitive to the tail of the probability distribution function (PDF) of alignment angle $|\boldsymbol{p} \cdot \boldsymbol{e}_i|$ than the first moment $\langle |\boldsymbol{p} \cdot \boldsymbol{e}_i| \rangle$, we provide both $\langle |\boldsymbol{p} \cdot \boldsymbol{e}_i| \rangle$ and $\langle (\boldsymbol{p} \cdot \boldsymbol{e}_i)^2 \rangle$

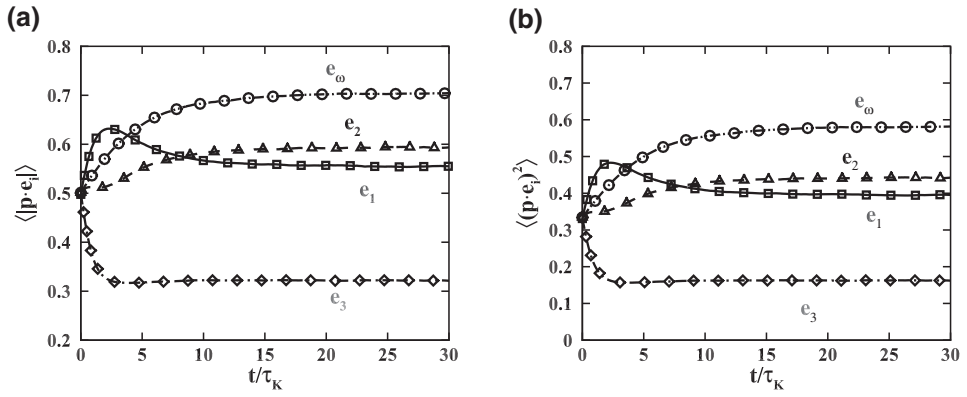

Figure 1. Alignment of rod-like particles ($\alpha = 100$) in isotropic turbulent flow: evolution alignment of $\boldsymbol{p}$ with the eigenvalues of strain, $\boldsymbol{e}_i$, and the direction of vorticity, $\boldsymbol{e}_\omega$, with time. (a) $\langle|\boldsymbol{p}\cdot\boldsymbol{e}_i|\rangle$, (b) $\langle(\boldsymbol{p}\cdot\boldsymbol{e}_i)^2\rangle$.

versus time and their time-average mean value at the stationary state in Figure 1 and Table 1. The results by Pumir and Wilkinson [9] are used to validate our result in Table 1. Figure 1 shows the evolution of the cosine of the angle between the orientation of the rod-like particles, $\boldsymbol{p}$, and the direction vectors, $\boldsymbol{e}_i$, of the velocity gradient tensor elements with time in DNS with $R_\lambda = 65$. At short times, the orientation vector $\boldsymbol{p}$ tends to align with the largest eigendirection of the strain and becomes perpendicular to the smallest eigendirection of the strain, as expected. However, as it gradually reaches the statistically stationary level, the alignment of the orientation vector $\boldsymbol{p}$ and the eigenvector $\boldsymbol{e}_i$ shows an interesting result: the alignment between $\boldsymbol{p}$ and $\boldsymbol{e}_1$ is reduced due to the trapping of rod-like particles by the vortex; thus, there is a much stronger alignment between $\boldsymbol{p}$ and $\boldsymbol{e}_\omega$. Moreover, the correlation between $\boldsymbol{p}$ and $\boldsymbol{e}_2$ implies that there is a strong alignment between $\boldsymbol{e}_\omega$ and $\boldsymbol{e}_2$, as has been proven by Ashurst et al. [38]. The constant mean values of the alignment of rod-like particles are listed in Table 1, with a group of data from Pumir and Wilkinson [9] provided for comparison, and the two sets of results well agree with each other. At the same time, we plot the PDF of $|\boldsymbol{p}\cdot\boldsymbol{e}_i|$ in Figure 2, which clearly demonstrates the preferential alignment between $\boldsymbol{p}$ and $\boldsymbol{e}_2$, $\boldsymbol{e}_\omega$. At $|\boldsymbol{p}\cdot\boldsymbol{e}_i| \to 1$, the PDFs of $|\boldsymbol{p}\cdot\boldsymbol{e}_2|$ and $|\boldsymbol{p}\cdot\boldsymbol{e}_\omega|$ are much large.

Finally, we investigate the mean square rotation rate, or the rotational energy, as a function of the aspect ratio by performing two sets of simulations with $R_\lambda = 65$ and 205. We can observe from Figure 3 that the variation of the curve of the rotational energy looks like the letter 'z' along the axis of the aspect ratio. When $\alpha \ll 1$, the rotational energy of the disk-like particles is much larger than that of the spheres ($\alpha = 1$), whereas the rotational energy of the rod-like particles ($\alpha \gg 1$) is much smaller than that of the spheres. The values of rotational energy are slightly dependent on the Reynolds number, and we obtain

Table 1. Statistics characterising the alignment of rod-like particles ($\alpha = 100$). X denotes $\boldsymbol{p}\cdot\boldsymbol{e}_i$ and data with $\alpha \to \infty$ from Pumir and Wilkinson.[9]

	$\boldsymbol{p}\cdot\boldsymbol{e}_1$	$\boldsymbol{p}\cdot\boldsymbol{e}_2$	$\boldsymbol{p}\cdot\boldsymbol{e}_3$	$\boldsymbol{p}\cdot\boldsymbol{e}_\omega$
$\langle\|X\|\rangle$, $\alpha \to \infty$, Ref. [9]	0.55	0.59	0.32	0.70
$\langle\|X\|\rangle$, $\alpha = 100$	0.55	0.60	0.32	0.70
$\langle(X)^2\rangle$, $\alpha \to \infty$, Ref. [9]	0.39	0.44	0.17	0.58
$\langle(X)^2\rangle$, $\alpha = 100$	0.39	0.45	0.16	0.58

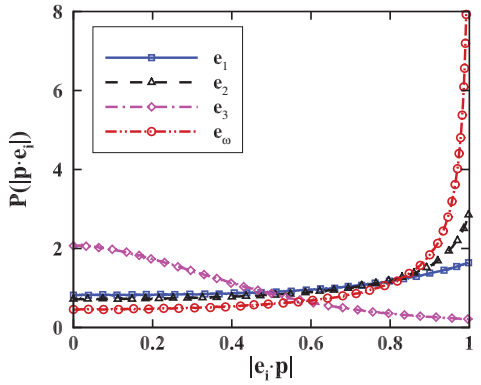

Figure 2. PDF of alignment between the rod-like particles ($\alpha = 100$) and velocity gradient tensors. $\boldsymbol{e}_i$, eigenvectors of strain tensor; $\boldsymbol{e}_\omega$, direction of vorticity; $\boldsymbol{p}$, a unit vector aligned with the axis of a rod-like particle.

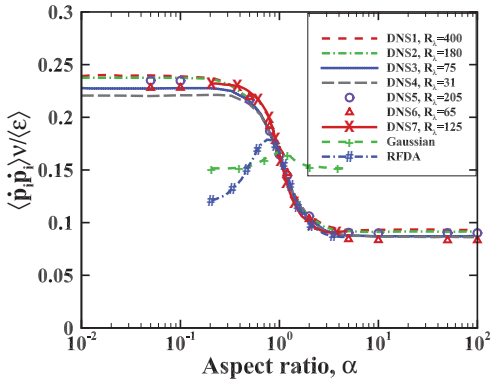

Figure 3. Mean square rotation rate against the aspect ratio. DNS1-4: DNS results from Parsa et al. [10]; DNS5-6: present DNS results; DNS7, Gaussian and RFDA: DNS and modelling results from Chevillard and Meneveau [39].

results consistent with those from Parsa et al. [10] and the DNS result from Chevillard and Meneveau [39]. The results of the two Lagrangian stochastic models, namely, the Gaussian process and recent fluid deformation approximation (RFDA) for velocity gradient tensor at full scale are also plotted for comparison. It is observed that all DNS results collapse well, while the Gaussian model is only valid for spherical particles at $\alpha = 1$, and the RFDA model behaves well for rod-like particles ($\alpha \gg 1$). More discussions on the rotational energy versus aspect ratio are presented in the next subsection.

3.2. Alignment of ellipsoidal particles with the eigenvectors of strain rate tensor and the vorticity vector

When considering the alignment of particles with different shapes or aspect ratios, we will find an interesting result in Figure 4. The rod-like particles tend to be parallel to $\boldsymbol{e}_2$ and $\boldsymbol{e}_\omega$, while the disk-like particles tend to align with $\boldsymbol{e}_3$ and to be perpendicular to $\boldsymbol{e}_2$ and $\boldsymbol{e}_\omega$. Here, we shall explain the different alignment of the rod- and disk-like particles. Because

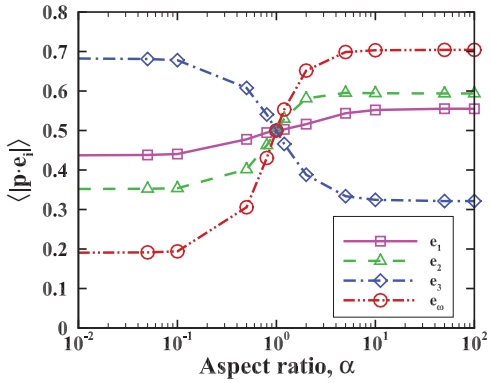

Figure 4. Alignment of ellipsoidal particles against the aspect ratio. The orientation vectors of disk-like particles tend to align with the directions perpendicular to the orientation vectors of rod-like particles.

we have known that the non-linear term in Equation (8) does not influence the rotational dynamics of the particles in Section 2, the solution of Jeffery's equation can also be obtained from $\boldsymbol{p}(t) = \boldsymbol{q}(t)/|\boldsymbol{q}(t)|$, where $\boldsymbol{q}$ is the unnormalised orientation vectors, its dependence on Ω and $\boldsymbol{S}$ can be written as $\dot{\boldsymbol{q}} = \Omega\boldsymbol{q} + \frac{\alpha^2-1}{\alpha^2+1}\boldsymbol{S}\boldsymbol{q}$. In the limiting cases, the equations of $\boldsymbol{q}$ for rod-like particles ($\alpha \to \infty$) and disk-like particles ($\alpha \to 0$) become

$$\dot{\boldsymbol{q}}_{\text{rod}} = \boldsymbol{A}(t)\boldsymbol{q}_{\text{rod}}, \tag{12}$$

$$\dot{\boldsymbol{q}}_{\text{disk}} = -\boldsymbol{A}^T(t)\boldsymbol{q}_{\text{disk}}, \tag{13}$$

where $\boldsymbol{A}$ is the velocity gradient tensor, $\boldsymbol{A} = \boldsymbol{S} + \Omega$, and $\boldsymbol{A}^T$ is the transpose of $\boldsymbol{A}$. Equations (12) and (13) imply that the dynamics of the disk- and rod-like particles are determined by $\boldsymbol{A}(t)$ and $-\boldsymbol{A}^T(t)$, respectively. Therefore, the eigenvalues of $\boldsymbol{A}$ (or $-\boldsymbol{A}^T$) directly influence the behaviours of $\boldsymbol{q}_{\text{rod}}$ (or $\boldsymbol{q}_{\text{disk}}$). There are three possible situations for the alignment of a rod-like particle with the eigenvector.[6] If there are three real eigenvalues, then $\boldsymbol{q}_{\text{rod}}$ aligns with the eigenvector corresponding to the largest eigenvalue. If there are one positive real eigenvalue and two complex conjugate eigenvalues, $\boldsymbol{q}_{\text{rod}}$ aligns with the eigenvector corresponding to the real eigenvalue. Otherwise, if the real eigenvalue is non-positive, $\boldsymbol{q}_{\text{rod}}$ rotates in the plane spanned by the real and imaginary parts of the complex eigenvector. Because the eigenvalues of $-\boldsymbol{A}^T$ and $\boldsymbol{A}$ have opposite signs, the order of eigenvalues from maximum value to minimum value is opposite, thus, disk-like particles tend to align with the directions perpendicular to the orientation vectors of rod-like particles, as shown in Figure 4. The alignment between the rod-like particles and the vorticity has been attributed to the similarities between the equations of motion (12) and (14) for rod-like particles and vorticity, and the additional viscous term in Equation (14) will slightly weaken the alignment between the rod-like particles and the vorticity,[9] as shown in Figure 1,

$$\dot{\boldsymbol{\omega}} = \boldsymbol{A}(t)\boldsymbol{\omega} + \nu\Delta^2\boldsymbol{\omega}. \tag{14}$$

As a result, the orientation vector of a rod-like particle tends to align with the vorticity vector, and the preferential alignment with vorticity will weaken the rotation of the rod-like particle, which leads to a lower rotational energy, whereas the orientation vector

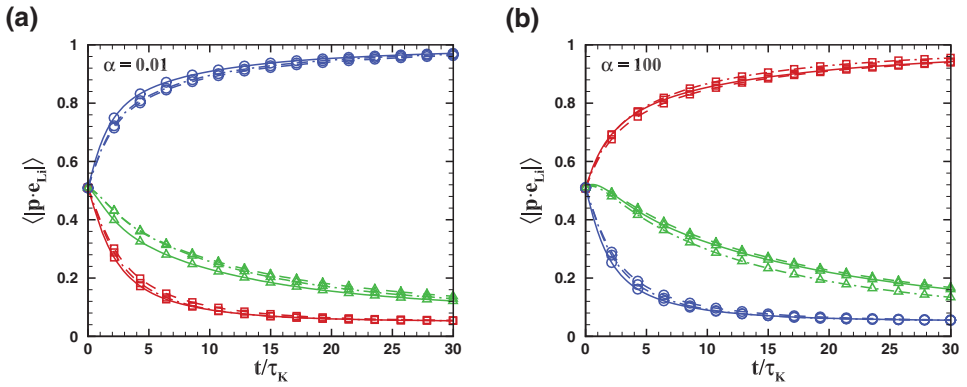

Figure 5. The alignment of the orientation vector $\boldsymbol{p}$ of ellipsoidal particles with respect to the eigenvectors $\boldsymbol{e}_{Li}$ ($i = 1,2,3$) of the left Cauchy–Green strain tensor $\boldsymbol{C}^{(L)}$. (a) Plots the alignment of disk-like particles, and (b) plots the alignment of rod-like particles. For all subfigures, $\boldsymbol{e}_{L1}$, $\boldsymbol{e}_{L2}$, and $\boldsymbol{e}_{L3}$ represented by the symbols 'square', 'triangle' and 'circle' correspond to the largest, intermediate and smallest eigenvalues of $\boldsymbol{C}^{(L)}$. The solid lines, dashed lines and dash-dotted lines show the results from DNS, LES and LES plus SDE.

of a disk-like particle tends to be perpendicular to the vorticity vector, and the perpendicular alignment will strengthen the rotation of the disk-like particle, and thus increase the rotational energy, as shown in Figure 3.

3.3. Alignment of ellipsoidal particles with Lagrangian fluid stretching direction

An alternative method to characterise the orientation of rod-like particles is Lagrangian fluid stretching, which can be described using the left Cauchy–Green tensor $\boldsymbol{C}^{(L)}$ [40],

$$\boldsymbol{C}^{(L)} = \boldsymbol{F}\boldsymbol{F}^{T}, \tag{15}$$

where $F_{ij} = (\partial x_{p,i}/\partial x_{0,j})$ is the deformation gradient tensor at $\boldsymbol{x}_p$ with respect to $\boldsymbol{x}_0$. The evolution equation of $\boldsymbol{F}$ can be obtained by differentiating Equation (7) with respect to $\boldsymbol{x}_0$,

$$\dot{\boldsymbol{F}} = \boldsymbol{A}(t)\boldsymbol{F}, \tag{16}$$

the initial condition is chosen as $F_{ij}(0) = \delta_{ij}$.

In this subsection, we shall investigate the alignment of ellipsoidal particles with Lagrangian stretching direction in DNS, LES and LES plus SDE (details about the SDE model for the SGS velocity gradient will be given in Section 3.5.1). Figure 5 shows the alignment of disk- and rod-like particles with the Lagrangian fluid stretching directions. Since the initial orientations of the ellipsoidal particles are randomly distributed, the alignments of the particles with each Lagrangian stretching direction start at approximately 0.5, and they finally approach different constants. In Figure 5(a), the alignment of the disk-like particles with $\boldsymbol{e}_{L3}$ is very strong; while in Figure 5(b), the rod-like particles tend to align with $\boldsymbol{e}_{L1}$, which is consistent with the results from Ni et al. [40]. The reason that disk- and rod-like particles tend to align with the smallest and the largest eigenvalues is due to the opposite order of eigenvectors in $-\boldsymbol{A}^{T}$ and $\boldsymbol{A}$ in Equations (12) and (13), which has been given in Section 3.2. It is interesting that the alignments of the ellipsoidal particles with the

Lagrangian stretching direction are insensitive to the changes of the velocity gradient tensor: For each Lagrangian stretching direction, the corresponding curves among DNS, LES and LES plus SDE overlap together. This phenomenon is owing to the same form of the equations of disk- and rod-like particles, Equations (12) and (13), as the equation of deformation gradient tensor, Equation (16). Since the orientation of the ellipsoidal particles and the deformation gradient tensor are passive vectors determined by the velocity gradient tensor, the changes of $\boldsymbol{A}$ would not influence the alignment between them. Therefore, the alignment of the ellipsoidal particles with the Lagrangian stretching would keep the same for different velocity gradient tensor, and it cannot reflect the effects of SGS motions or models on the orientational dynamics of the ellipsoidal particles.

3.4. Effects of SGS motions on orientational and rotational dynamics

In isotropic turbulence, the rotation of ellipsoidal particles is determined by the velocity gradient along the particle trajectories. Because the vorticity in Equation (14) or the enstrophy is largely accumulated at small scales, which is much underpredicted in LES, it raises a challenge to predict the rotational dispersion of ellipsoidal particles using the LES. In this subsection, we shall examine the alignment and rotation of ellipsoidal particles in LES.

Figure 6 shows the alignment of the disk- ($\alpha = 0.01$) and rod-like particles ($\alpha = 100$) between the axial vectors $\boldsymbol{p}$ and the elements of the velocity gradient direction from DNS, FDNS and LES. Because the orientation vectors of disk-like particles tends to align with the directions perpendicular to the orientation vectors of rod-like particles as shown in Figure 4, we discuss the rod-like particle cases in Figure 6(e)–6(h) first. We find that the alignment of the rod-like particles in both FDNS and LES has a large difference from that in DNS, which is easy to understand because neither FDNS nor LES resolves the SGS velocity fluctuations. The preferential alignment between $\boldsymbol{p}$ and $\boldsymbol{e}_\omega$ in LES and FDNS is much weaker than that in DNS. This is because the strong vorticity at small scales is filtered out and the vortex trapping of rod-like particle is thus weakened. In this study, the FDNS method is considered as an ideal LES method without any SGS model, and the errors mainly come from the filtering operation. However, the additional viscous dissipation from the eddy viscosity model in LES increases the coherence of the flows. As shown by Pumir and Wilkinson [9], the viscous term in Equation (14) influences the correlation between the orientation vector of the rod-like particle and the vorticity vector. Hence, the additional SGS eddy viscosity in LES will further weaken the alignment between the rod-like particle and the vorticity. Because the filtering operation is the major factor that affects the alignment of the particles, the effect of the additional SGS eddy viscosity in LES on the alignment of the particles is relatively small. For disk-like particles, the filtering operation leads a similar error to their alignment with the eigenvectors of the fluid velocity gradient tensor, as shown in Figure 6(a)–6(d), and the effects of the SGS eddy viscosity in LES on the alignment of disk-like particles are also very small.

Now, we study the mean square rotation rate of the ellipsoidal particles, as shown in Figure 7. The curves of FDNS and LES are both under the curve of DNS, which indicates that the filtering operation decreases the vorticity of the flow and reduces the rotational energy. Figure 7 also reflects that the curve from LES is lower than that from FDNS. Although the alignment of the ellipsoidal particles is similar in FDNS and LES, the vorticity or enstrophy in LES is much smaller than that in FDNS due to the over-dissipation of the

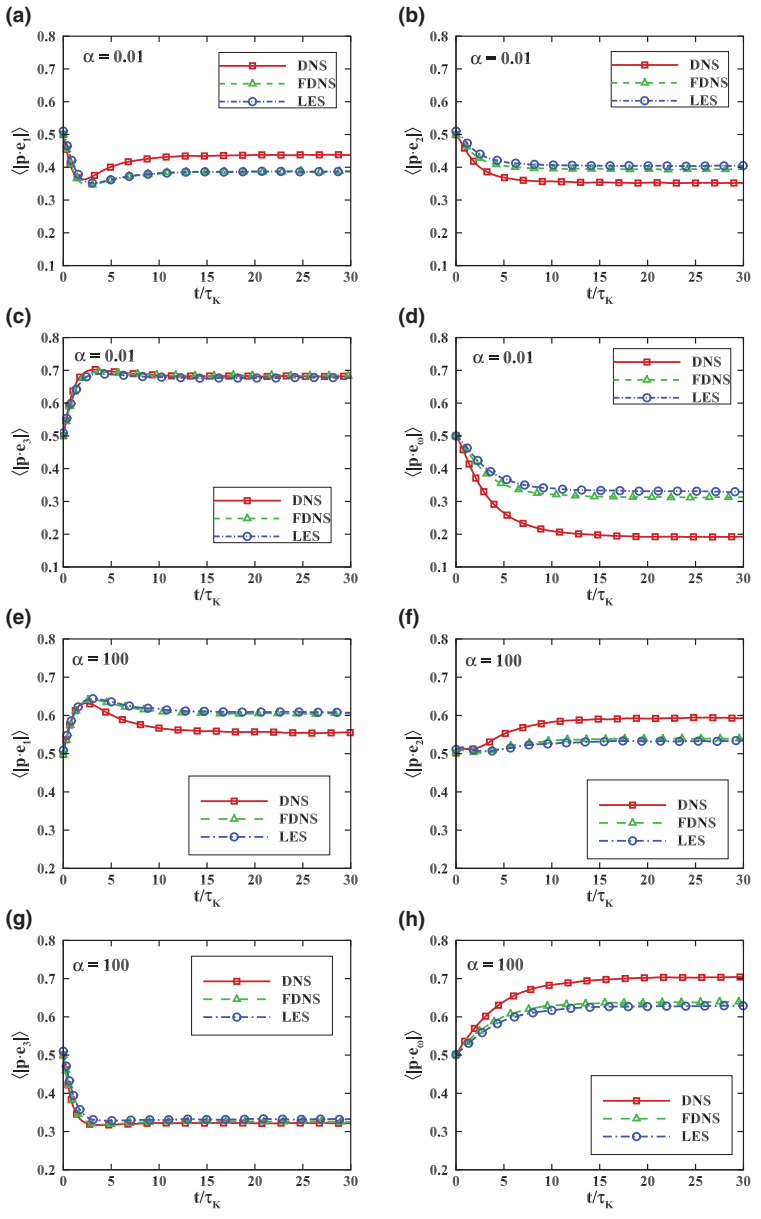

Figure 6. Comparison of alignment of the disk- and rod-like particles among DNS, FDNS and LES. (a)–(d) Plot the alignment of disk-like particles, and (e)–(h) plot the alignment of rod-like particles. FDNS and LES have the approximate alignment of ellipsoidal particles and exhibit a large difference in the alignment from DNS.

SGS eddy viscosity model. In conclusion, the loss of vorticity or enstrophy in LES results in large errors in the orientational and rotational statistics of the ellipsoidal particles.

3.5. Applications of SGS models to LES of orientation and rotation of the ellipsoidal particles

The SGS motions of fluid are unresolved in LES, which leads to large errors in the rotational statistics of the ellipsoidal particles, as demonstrated in Section 3.4. Thus, an SGS model

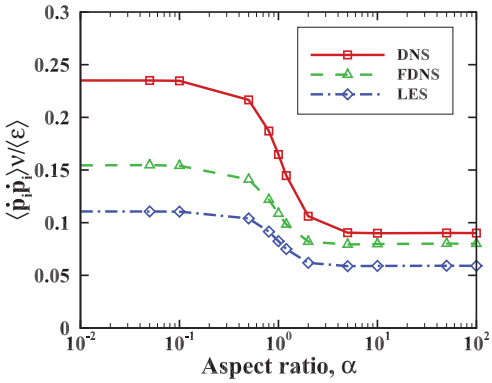

Figure 7. Comparison of mean square rotation rate against aspect ratio among DNS, FDNS and LES. Both FDNS and LES yield smaller rotation rates than DNS, while LES has the smallest values. The average energy dissipation rate $\langle \varepsilon \rangle$ is from DNS.

to account for the effects of SGS motions on rotational dispersion of ellipsoidal particles is required. Two types of SGS models are commonly used in LES of particle-laden turbulence. One is the SGS stochastic model, which can be used to reconstruct the SGS fluctuations.[25] The other is based on ADM, which can recover the SGS kinetic energy near the cut-off wavenumbers.[29] In this subsection, we describe the effects of the SGS-SDE model and the SGS-ADM model on the orientational and rotational statistics.

3.5.1. *A stochastic model for the SGS velocity gradient tensor*

To compensate for the effect of the SGS motions on the orientational and rotational statistics of ellipsoidal particles, the construction of an SGS model is essential. However, a stochastic SGS model for fluid velocity will make the velocity field non-differential so that the velocity gradient tensor required in Equation (8) is unavailable. Therefore, we shall directly build a stochastic model for the SGS velocity gradient tensor along the trajectories of the particles.

Several Lagrangian stochastic models for the velocity gradient tensor in turbulent flows have been proposed.[41–43] Chevillard and Meneveau [39] studied the orientational dynamics by using DNS and several models for velocity gradient tensor, as shown in Figure 3. The Gaussian model is based on a linear Ornstein–Uhlenbeck process, and it yields a poor prediction of the rotation rate except for spherical particles. The RFDA Lagrangian stochastic model proposed by Chevillard and Meneveau [42] yields accurately predictions of the rotation rate for rod-like particles. Pumir and Wilkinson [9] proposed a more refined Gaussian processes by considering an Ornstein–Uhlenbeck process for $\boldsymbol{A}$. The correlation time scales for the strain rate and the rotation rate are respectively provided according to the fact that the former is shorter than the latter in isotropic turbulent flows. Both the RFDA model and the refined Gaussian model have been previously applied to the full velocity gradient tensor.[9,39] In this study, we will construct a Lagrangian stochastic model for the SGS velocity gradient tensor based on the refined Gaussian process.

The statistics of the SGS velocity gradient tensor A'_{ij} can be obtained from DNS and FDNS,

$$A'_{ij} = A_{ij} - \bar{A}_{ij}, \tag{17}$$

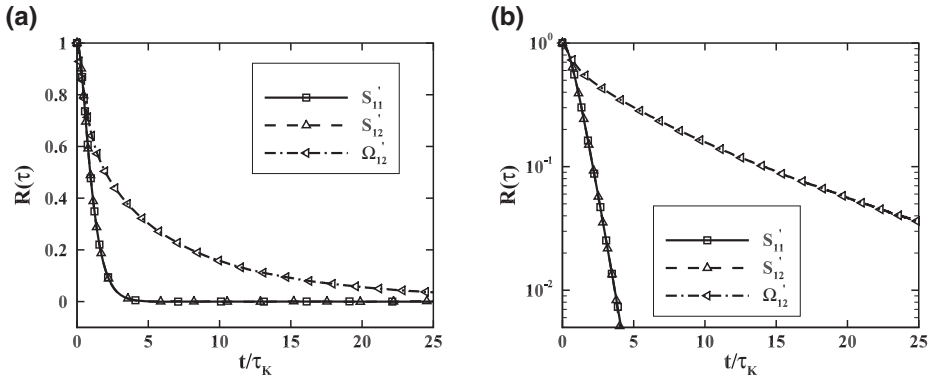

Figure 8. Correlation functions of the elements of the SGS velocity gradient tensor against normalised time t/τ_K. The decay rate of the strain rate tensor is much larger than that of the rotation rate.

where A_{ij} is the velocity gradient tensor from DNS, and $\bar{A}_{ij}$ from FDNS. The auto-correlation functions of the components of strain and vorticity are shown in Figure 8, $R(\tau) = \langle X(t)X(t+\tau)\rangle/\langle X^2(t)\rangle$, where X denotes a component of the strain or vorticity. We can observe two straight lines on the semi-log graph from Figure 8(b), which implies that the elements of the SGS velocity gradient can be well approximated by exponential functions. Therefore, we can follow the idea of Pumir and Wilkinson [9] to propose an SGS-SDE model for the elements of the SGS velocity gradients. It must be noted that the model built by Pumir and Wilkinson [9] is based on the full scales of the flow, whereas our model is only based on the fluid flow at SGSs.

The components of the SGS vorticity and strain can then be modelled as

$$\mathrm{d}\Omega'_{ij} = -\frac{\mathrm{d}t}{\tau_v}\Omega'_{ij} + \sqrt{2D_v}\xi_{ij}(t), \tag{18}$$

$$\mathrm{d}S'_{ij} = -\frac{\mathrm{d}t}{\tau_s}S'_{ij} + \sqrt{2D_o}\eta_{ij}(t), \tag{19}$$

$$\mathrm{d}S'_{ii} = -\frac{\mathrm{d}t}{\tau_s}S'_{ii} + \sqrt{2D_d}\left[\eta_{ii}(t) - \frac{1}{3}\sum_{j=1}^{3}\eta_{jj}\right], \tag{20}$$

where τ_v is the integral time scale of the component of the SGS vorticity, $D_v = \sigma_v^2/\tau_v$, the diffusion coefficients, $\sigma_v^2 = \langle\Omega_{ij}(0)\Omega_{ij}(0)\rangle$, τ_s is the integral time scale of the component of strain, D_o and D_d are the diffusion coefficients of the off-diagonal and diagonal elements of the strain, respectively ($D_v = 5.36$, $\tau_v = 3.67 \times 10^{-1}$, $D_d = 2.21$, $D_o = 1.90$ and $\tau_s = 7.74\times10^{-2}$ in this paper), and ξ and η are white-noise signals with $\langle\xi(t)\rangle = 0$, $\langle\xi(t)\xi(t')\rangle = \mathrm{d}t$ and $\langle\eta(t)\rangle = 0$, $\langle\eta(t)\eta(t')\rangle = \mathrm{d}t$.

3.5.2. Approximate deconvolution methods

In LES, only the filtered velocity $\hat{\bar{\boldsymbol{u}}}$ is available, so the improved fluid velocity $\hat{\boldsymbol{u}}^*$ can be calculated by applying the deconvolution operator $\hat{G}^{-1}$ to $\hat{\bar{\boldsymbol{u}}}$,

$$\hat{\boldsymbol{u}}^* = \hat{G}^{-1}\hat{\bar{\boldsymbol{u}}}, \tag{21}$$

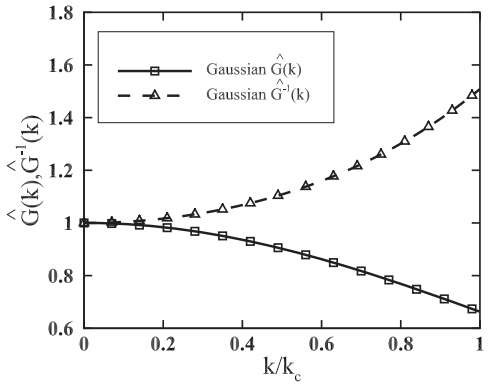

Figure 9. The one-dimensional Gaussian filter and its approximate inverse against normalised wavenumber k/k_c. The approximate inverse $\hat{G}^{-1}$ can increase the Fourier coefficients near the cut-off wavenumber by approximately 50%.

where $\hat{G}$ is a filter function in spectral space, and

$$\hat{G}^{-1}(k) \simeq \sum_{n=0}^{N} \left(1 - \hat{G}(k)\right)^n. \tag{22}$$

As advised by Stolz and Adams [27], $N = 5$ is sufficient,

$$\hat{G}^{-1}(k) \simeq 6 - 15\hat{G}(k) + 20\hat{G}^2(k) - 15\hat{G}^3(k) + 6\hat{G}^4(k) - \hat{G}^5(k). \tag{23}$$

Substituting Equation (23) into Equation (21), the improved fluid velocity $\hat{\boldsymbol{u}}^*$ can be given by the repeated filtering of $\hat{\bar{\boldsymbol{u}}}$ from,

$$\hat{\boldsymbol{u}}^* \simeq 6\hat{\bar{\boldsymbol{u}}} - 15\hat{\bar{\bar{\boldsymbol{u}}}} + 20\hat{\bar{\bar{\bar{\boldsymbol{u}}}}} - 15\hat{\bar{\bar{\bar{\bar{\boldsymbol{u}}}}}} + 6\hat{\bar{\bar{\bar{\bar{\bar{\boldsymbol{u}}}}}}} - \hat{\bar{\bar{\bar{\bar{\bar{\bar{\boldsymbol{u}}}}}}}}. \tag{24}$$

The above filter $\hat{G}$ has to satisfy $|1 - \hat{G}| < 1$ and have an inverse. In this study, we choose a 3D Gaussian filter definition as follows:

$$\hat{G}(\boldsymbol{k}) = \begin{cases} \exp\left(-\frac{|\boldsymbol{k}|^2\Delta^2}{24}\right) & \text{if } |\boldsymbol{k}| < k_c, \\ 0 & \text{if } |\boldsymbol{k}| > k_c. \end{cases} \tag{25}$$

The one-dimension Gaussian filter and its inverse are plotted in Figure 9, where we can observe that the inverse filter is expected to increase the Fourier coefficients near the cut-off wavenumber.

3.5.3. *Effects of the SGS models on orientational and rotational dynamics*

The SGS-SDE model reconstructs the SGS fluctuations of the velocity gradient along the trajectories of the particles, whereas the ADM increases the accuracy of the flow field near the cut-off wavenumber, however, without recovering any motions at the scales smaller than

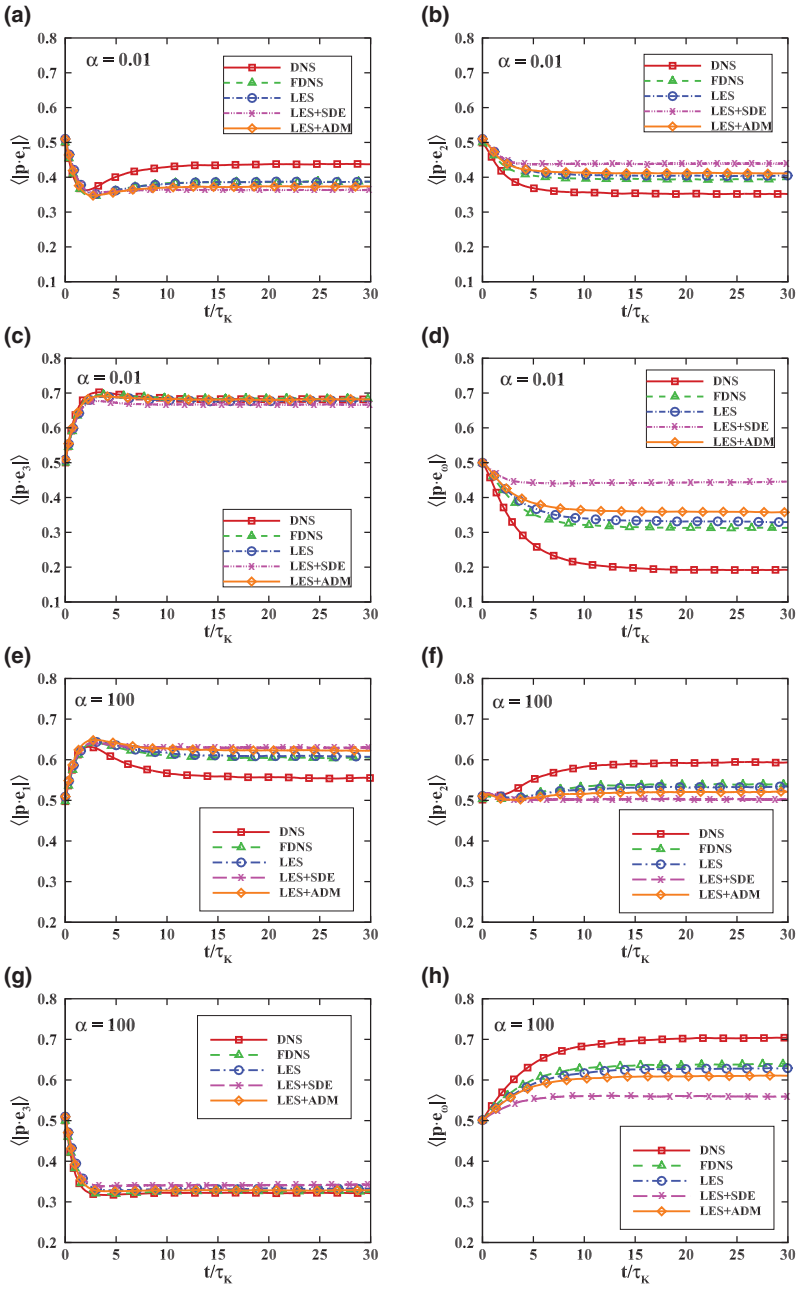

Figure 10. Comparison of the alignment of disk- and rod-like particles among DNS, FDNS, LES, LES plus SDE, and LES plus ADM. (a)–(d) Plot the alignment of disk-like particles, and (e)–(h) plot the alignment of rod-like particles. The SDE model introduces larger errors into the alignment of the ellipsoidal particles, whereas the ADM has little influence on the alignment of the ellipsoidal particles.

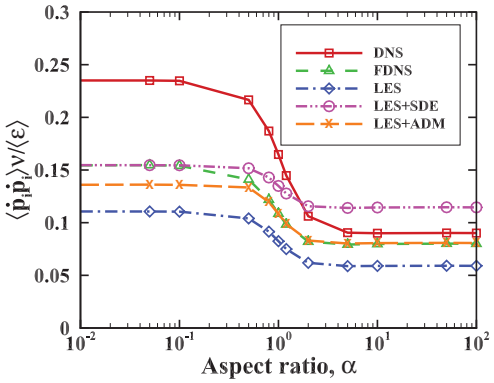

Figure 11. Comparison of the mean square rotation rate against the aspect ratio among DNS, FDNS, LES, LES plus SDE and LES plus ADM. The SDE model over-predicts the rotational energy of the rod-like particles, and the ADM significantly increases the rotational energy.

the filter width. It is expected that the influences of the two models on the orientational and rotational statistics of the ellipsoidal particles will be different. We consider the alignment statistics first.

Figure 10 shows the alignment of disk- and rod-like particles among DNS, FDNS, LES, LES plus SDE and LES plus ADM, where (a)–(d) plot the alignment of disk-like particles, and (e)–(h) plot the alignment of rod-like particles. We focus on the alignment of rod-like particles first. We find that the effects of LES plus ADM on the alignment of the rod-like particles are small, with the alignment of the rod-like particles between $\boldsymbol{p}$ and $\boldsymbol{e}_\omega$ being slightly smaller than that of LES. Equations (12) and (14) show that vorticity influences the alignment of rod-like particles. Since the ADM contributes little to the vorticity at small scales, the effects of the ADM on the alignment of the rod-like particles are small, as expected. However, the effects of the SGS-SDE model on the alignment are much larger than those of the ADM: the alignment between $\boldsymbol{p}$ and $\boldsymbol{e}_\omega$ is much smaller than that of LES. The reconstructed SGS velocity gradient in this model is white-noise information, it damages the correlation between $\boldsymbol{q}$ and $\boldsymbol{\omega}$. For disk-like particles, Figure 10(a)–10(d) show that the effects of the two models on these particles are similar to those on rod-like particles in the sense that the influence of ADM on the alignment is small while the influence of SGS-SDE model is much large. On the whole, neither of the models improves the alignment of disk- and rod-like particles.

Finally, we will examine the effects of the SGS motions on the rotation rate against the aspect ratio in Figure 11. When $\alpha \ll 1$, the SGS-SDE model improves the rotational energy, and when $\alpha \gg 1$, it over-predicts the rotational energy. The additional rotational energy comes from the introduction of the SGS fluctuations. Furthermore, the failure of preferential alignment with vorticity also increases the rotation rate of the rod-like particles. For ADM, it recovers the fluid enstrophy near the cut-off wavenumber, resulting in an improvement in rotational energy of particles.

4. Conclusions

The rotational dispersion and orientation distribution of ellipsoidal particles in isotropic turbulence are very important in many environmental and industrial flows. The rotational

motion of an ellipsoidal particle is determined by the fluid velocity gradient tensor along its trajectory, which is dominated by the small scales of turbulent flows. Therefore, large errors in the orientational and rotational statistics can be observed in LES due to the missing of SGS motions. We discuss the variation of the alignment of disk- and rod-like particles with the vorticity against the aspect ratio α. The opposite signs of the eigenvalues of the fluid velocity gradient tensor in the equations of motion of disk- and rod-like particles (Equations (12) and (13)) lead to a different alignment with vorticity, which results in the rod-like particles tending to align with the vorticity and the disk-like particles tending to be perpendicular to the vorticity, and disk-like particles have higher rotational energy than rod-like particles. The alignment of the disk- and rod-like particles with the Lagrangian stretching directions is studied. It is found that the alignment between these passive vectors is insensitive to the changes in velocity gradient tensor obtained by using DNS or LES, thus the Lagrangian stretching would not be used to examine the effects of the SGS motions and the Lagrangian stochastic models. We then study the effects of SGS motions on the alignment and rotation rate of the ellipsoidal particles. It is observed that the missing SGS motion especially the SGS vorticity or enstrophy in LES weakens the alignment with the vorticity and reduces the rotational energy. Furthermore, we compare the statistical results of two SGS models, i.e. the SGS-SDE model and the ADM model, for particles. The SGS-SDE model fails to produce the proper alignment between the orientation vector of the ellipsoidal particles and the velocity gradient tensor, and it over-predicts the rotational energy of the rod-like particles. The ADM model improves the rotational energy although has little effect on the improvement in the alignment. In the further work, we will try to construct the model for the SGS velocity gradient tensor based on the RFDA Lagrangian stochastic model to improve the rotational statistics of ellipsoidal particles by using LES method.

Acknowledgements

This work was supported by the 973 Program of China (grant number 2013CB834100), the National Natural Science Associate Foundation (NSAF) of China (grant number U1230126), the National Natural Science Foundation of China (NSFC) (grant numbers 11232011 and 11472277). Guodong Jin benefitted from the hospitality of the Nordic Institute for Theoretical Physics under the auspices of the program 'Dynamics of Particles in Flows: Fundamentals and Applications' in June 2014 in Sweden. The computation was performed on Tianhe-I supercomputer at Tianjin, China. The two anonymous reviewers are much appreciated for the constructive suggestions to improve the manuscript.

Disclosure statement

No potential conflict of interest was reported by the authors.

Funding

This work was supported by the 973 Program of China [grant number 2013CB834100]; the National Natural Science Associate Foundation (NSAF) of China [grant number U1230126]; the National Natural Science Foundation of China (NSFC) [grant number 11232011], [grant number 11472277].

References

[1] Pedley TJ, Kessler JO. Hydrodynamic phenomena in suspensions of swimming microorganisms. Annu Rev Fluid Mech. 1992;24:313–358.
[2] Guasto JS, Rusconi R, Stocker R. Fluid mechanics of planktonic microorganisms. Annu Rev Fluid Mech. 2012;44:373–400.
[3] Pécseli HL, Trulsen J, Fiksen Ø. Predator-prey encounter and capture rates for plankton in turbulent environments. Progr Oceanogr. 2012;101:14–32.
[4] Lundell F, Söderberg LD, Alfredsson PH. Fluid mechanics of papermaking. Annu Rev Fluid Mech. 2011;43:195–217.
[5] Jeffery GB. The motion of ellipsoidal particles immersed in a viscous fluid. Proc R Soc A. 1922;102(715):161–179.
[6] Bretherton FP. The motion of rigid particles in a shear flow at low Reynolds number. J Fluid Mech. 1962;14(2):284–304.
[7] Shin M, Koch DL. Rotational and translational dispersion of fibres in isotropic turbulent flows. J Fluid Mech. 2005;540:143–173.
[8] Guala M, Liberzon A, Luthi B, et al.. Stretching and tilting of material lines in turbulence: the effect of strain and vorticity. Phys Rev E. 2006;73:036303.
[9] Pumir A, Wilkinson M. Orientation statistics of small particles in turbulence. New J Phys. 2011;13:093030.
[10] Parsa S, Calzavarini E, Toschi F, et al.. Rotation rate of rods in turbulent fluid flow. Phys Rev Lett. 2012;109:134501.
[11] Parsa S, Voth GA. Inertial range scaling in rotations of long rods in turbulence. Phys Rev Lett. 2014;112:024501.
[12] Einarsson J, Angilella JR, Mehlig B. Orientational dynamics of weakly inertial axisymmetric particles in steady viscous flows. Physica D. 2014;278–279:79–85.
[13] Zhao LH, Andersson HI, Gillissen JJJ. On inertial effects of long fibers in wall turbulence: fiber orientation and fiber stresses. Acta Mech. 2013;224:2375–2384.
[14] Challabotla NR, Zhao LH, Andersson HI. Orientation and rotation of inertial disk particles in wall turbulence. J Fluid Mech. 2015;766:1–11.
[15] Moin P. Advances in large eddy simulation methodology for complex flows. Int J Heat Fluid Flow. 2002;23:710–720.
[16] Jin GD, He GW, Wang LP. Large-eddy simulation of turbulent collision of heavy particles in isotropic turbulence. Phys Fluids. 2010;22:055106.
[17] Yang Y, He GW, Wang LP. Effects of subgrid-scale modeling on Lagrangian statistics in large-eddy simulation. J Turbulence. 2008;9(8):1–24.
[18] Jin GD, He GW, Wang LP, et al.. Subgrid scale fluid velocity timescales seen by inertial particles in large-eddy simulation of particle-laden turbulence. Int J Multiphase Flow. 2010;36:432–437.
[19] Jin GD, He GW. A nonlinear model for the subgrid timescale experienced by heavy particles in large eddy simulation of isotropic turbulence with a stochastic differential equation. New J Phys. 2013;15:035011.
[20] He GW, Rubinstein R, Wang LP. Effects of subgrid-scale modeling on time correlations in large eddy simulation. Phys Fluids. 2002;14:2186–2193.
[21] He GW, Zhang JB. Elliptic model for space-time correlations in turbulent shear flows. Phys Rev E. 2006;73:055303.
[22] Zhao X, He GW. Space-time correlations of fluctuating velocities in turbulent shear flows. Phys Rev E. 2009;79:046316.
[23] Olson JA, Kerekes RJ. The motion of fibres in turbulent flow. J Fluid Mech. 1998;377:47–64.
[24] Kuczaj AK, Geurts BJ. Mixing in manipulated turbulence. J Turbulence. 2006;7:1–28.
[25] Simonin O, Deutsch E, Minier JP. Eulerian prediction of the fluid/particle correlated motion in turbulent two-phase flows. Appl Sci Res. 1993;51:275–283.
[26] Geurts BJ. Inverse modeling for large-eddy simulation. Phys Fluids. 1997;9:3585–3588.
[27] Stolz S, Adams NA. An approximate deconvolution procedure for large-eddy simulation. Phys Fluids. 1999;11:1699–1701.

[28] Stolz S, Adams NA, Kleiser L. An approximate deconvolution model for large-eddy simulation with application to incompressible wall-bounded flows. Phys Fluids. 2001;13:997–1015.
[29] Kuerten JGM. Subgrid modeling in particle-laden channel flow. Phys Fluids. 2006;18:025108.
[30] Michałek WR, Kuerten JG, Zeegers JCH, et al.. A hybrid stochastic-decovolution model for large-eddy simulation of particle-laden flow. Phys Fluids. 2013;25:123302.
[31] Rosa B, Parishani H, Ayala O, et al.. Kinematic and dynamic pair collision statistics of sedimenting inertial particles relevant to warm rain initiation. J Phys: Conf Ser. 2011;27:1921–1936.
[32] Chen JC, Jin GD, Zhang J. Lagrangian statistics in isotropic turbulent flows with deterministic and stochastic forcing schemes. Acta Mech Sinica. 2015;31:25–31.
[33] Chollet JP, Lesieur M. Parameterization of small scales of three dimensional isotropic turbulence utilizing spectral closure. J Atmos Sci. 1981;38:2747–2757.
[34] Chollet JP. Two-point closure used for a sub-grid scale model in large eddy simulations. In: Durst F, Launder B, editors. Turbulent shear flows 4. Berlin: Springer; 1985. p. 62–72.
[35] Ayala O, Parishani H, Chen L, et al.. DNS of hydrodynamically interacting droplets in turbulent clouds: parallel implementation and scalability analysis using 2D domain decomposition. Comput Phys Commun. 2014;185:3269–3290.
[36] Press WH, Teukolsky SA, Vetterling WT, et al.. Numerical recipes in fortran: the art of scientific computing. Cambridge: Cambridge University Press; 1992.
[37] Marcus GG, Parsa S, Kramel S, et al.. Measurements of the solid-body rotation of anisotropic particles in 3D turbulence. New J Phys. 2014;16:102001.
[38] Ashurst WT, Kerstein AR, Kerr RM, et al.. Alignment of vorticity and scalar gradient with strain rate in simulated Navier-Stokes turbulence. Phys Fluids. 1987;30:2343–2353.
[39] Chevillard L, Meneveau C. Orientation dynamics of small, triaxial-ellipsoidal particles in isotropic turbulence. J Fluid Mech. 2013;737:571–596.
[40] Ni R, Ouellette NT, Voth GA. Alignment of vorticity and rods with Lagrangian fluid stretching in turbulence. J Fluid Mech. 2014;743:1–10.
[41] Girimaji SS, Pope SB. Material-element deformation in isotropic turbulence. J Fluid Mech. 1990;220:427–458.
[42] Chevillard L, Meneveau C. Lagrangian dynamics and statistical geometric structure of turbulence. Phys Rev Lett. 2006;97:174501.
[43] Meneveau C. Lagrangian dynamics and models of the velocity gradient tensor in turbulent flows. Annu Rev Fluid Mech. 2011;43:219–245.